

Periplasmic vestibule plays an important role for solute recruitment, selectivity, and gating in the Rh/Amt/MEP superfamily

Ugur Akgun^a and Shahram Khademi^{a,b,1}

^aDepartment of Biochemistry, and ^bDepartment of Molecular Physiology and Biophysics, Carver College of Medicine, University of Iowa, Iowa City, IA 52242-1109

Edited* by Robert M. Stroud, University of California, San Francisco, CA, and approved January 20, 2011 (received for review May 27, 2010)

AmtB, a member of the Rh/Amt/MEP superfamily, is responsible for ammonia transport in *Escherichia coli*. The ammonia pathway in AmtB consists of a narrow hydrophobic lumen in between hydrophilic periplasmic and cytoplasmic vestibules. A series of molecular dynamics simulations (greater than 0.4 μ s in total) were performed to determine the mechanism of solute recruitments and selectivity by the periplasmic vestibule. The results show that the periplasmic vestibule plays a crucial role in solute selectivity, and its solute preferences follow the order of $\text{NH}_4^+ > \text{NH}_3 > \text{CO}_2$. Based on our results, NH_4^+ recruitment is initiated by its interaction with either E70 or E225, highly conserved residues located at the entrance of the vestibule. Subsequently, the backbone carbonyl groups at the periplasmic vestibule direct NH_4^+ to the conserved aromatic cage at the bottom of the vestibule (known as the Am1 site). The umbrella sampling simulations suggest that the conserved residue D160 is not directly involved in the ammonia conduction; rather its main function is to keep the structure of periplasmic vestibule intact. The MD simulations also revealed that two partially stacked phenyl rings of F107 and F215, separating the periplasmic vestibule from the hydrophobic lumen, flip open and closed simultaneously with a frequency of approximately 10^8 flipping events per second. These results show how the periplasmic vestibule selectively recruits NH_4^+ to the Am1 site, and also that the synchronized flipping of two phenyl rings potentially facilitates the solute transition from the periplasmic vestibule to the hydrophobic lumen in the Rh/Amt/MEP superfamily.

ammonia channel | membrane proteins | molecular dynamic simulations

The transport of ammonia across biological membranes is a fundamental process in all domains of life (1). In an aqueous solution, NH_3 and NH_4^+ (collectively referred to as Am) are in equilibrium with a pK_a of 9.25. At low Am concentrations (such as ~ 10 μ M), where the lipid bilayer diffusion for NH_3 is not sufficient to support microorganisms' needs for nitrogen uptake, Am transport is carried out by members of the Amt/Rh/MEP membrane protein superfamily. Members of the Amt/Rh/MEP family are found in yeast (*Methylammonium/ammonium Permease* or MEP) (2), plants (so-called *Ammonium transporter* or Amt) (3), bacteria (AmtB) (4), and mammals (Rh proteins) (5, 6). In mammalian Rh proteins (such as RhAG, RhBG, and RhCG) play a very important role in acid-base homeostasis (7–9). The measurements of Am permeation in red blood cells that express Rh proteins (10), in proteoliposomes reconstituted with AmtB (11) or Rh proteins (12), and in channel expressing *Xenopus* oocytes (13, 14) show that neutral NH_3 is the conducted species in Amt/Rh/MEP proteins. However, there is a report of electrogenic transport for some Amts from plants, suggesting NH_4^+ or $\text{NH}_3 + \text{H}^+$ could transit the channel in some members of this superfamily (15).

Since the original structures of AmtB from *Escherichia coli* were published (11, 16), multiple structures of members of the Amt/Rh/MEP family have been determined (17–22), and the structure of human RhCG is the latest one (22). The crystal struc-

ture of AmtB shows a homotrimer of three channels (11), which is the stable form of the protein in detergents (23) and in lipid bilayers (24). The structure of AmtB revealed a pathway for Am that includes periplasmic and cytoplasmic vestibules connected by a 20-Å-long hydrophobic lumen. The crystal structure of AmtB shows the connection between the periplasmic vestibule and the hydrophobic lumen is blocked by two partially stacked aromatic rings of the highly conserved residues F107 and F215. These phenyl rings are speculated to be flipped open upon Am passage (11). Based on the hydrophobic nature of the Am pathway, the differences in the electron density maps of AmtB structures with and without solutes, and also proteoliposome stopped-flow functional assays, Khademi et al. proposed a mechanism of Am conduction in the Amt/Rh/MEP family (11). According to this mechanism, NH_4^+ (the dominant species at physiologic pH) is recruited by periplasmic vestibule. As NH_4^+ enters the hydrophobic lumen, it releases its proton to water and passes through the lumen as neutral NH_3 . It has also been shown that AmtB and Rh proteins can conduct CO_2 , although to a lesser extent than that of Am (14, 25).

Although there are multiple reports of molecular dynamics (MD) simulations on the mechanism of solute conduction by AmtB (26–35), there are still major unanswered questions as follows: (i) How does the periplasmic vestibule recruit Am? (ii) What is the mechanism of solute (Am vs. CO_2) selectivity in AmtB? (iii) What is the role of the conserved residue D160 that is shown to be essential for AmtB activity (14, 36)? (iv) How do the phenyl rings of F107 and F215 gate the entrance of the lumen? In this paper, we used diverse MD simulation techniques to address these questions.

Results and Discussion

The Periplasmic Vestibule Prefers the Recruitment of NH_4^+ . The model used in our MD simulations includes a trimeric AmtB embedded into a solvated lipid bilayer of phosphatidylethanolamine (POPE) (Fig. S1). During an 84-ns equilibrium MD simulation for a system that includes 100 NH_4^+ and 106 Cl^- ions, NH_4^+ ions tended to remain more at the periplasmic side, whereas Cl^- ions tended to stay mainly on the cytoplasmic side. This is primarily due to the dipolar charge distribution of AmtB. We did not observe any recruitment of Cl^- by AmtB vestibules. However, five separate NH_4^+ recruitment events by the periplasmic vestibule were observed.

In each recruitment event, the NH_4^+ ion reached the aromatic cage formed by the phenyl rings of F107, F103, and W148 at the

Author contributions: S.K. designed research; U.A. performed research; U.A. and S.K. analyzed data; and U.A. and S.K. wrote the paper.

The authors declare no conflict of interest.

*This Direct Submission article had a prearranged editor.

¹To whom correspondence should be addressed. E-mail: shahram-khademi@uiowa.edu.

This article contains supporting information online at www.pnas.org/lookup/suppl/doi:10.1073/pnas.1007240108/-DCSupplemental.

the lipid bilayer, we did not see the CO_2 penetration in the regions covered by the cylindrical volume during our simulations (Fig. S5). Most likely longer simulations will show the penetration of CO_2 in this region as well. The drastic variations in the solutes' distributions were observed at the vicinity of the protein (Fig. 1B). Although the distributions of NH_3 molecules are similar to that of water molecules, the major deviations belong to NH_4^+ . NH_4^+ ions prefer to associate with the periplasmic side of AmtB. The highest deviations in the distribution of NH_4^+ are observed inside the periplasmic vestibule, with a peak at the Am1 site (Fig. 1B). The probability peak of 5.2% at Am1 is about 10 times higher than the average probability of finding a water molecule (used as a control) at that site ($0.4\% \pm 0.05\%$). The second highest probability peak belongs to NH_3 consistent with the finding that NH_3 can also be recruited by the vestibule (Fig. 1B).

We used the energy profiles of NH_4^+ and NH_3 conductions to estimate where NH_4^+ releases its proton in the channel and becomes NH_3 . The energy profiles for NH_4^+ and NH_3 conductions were calculated using nonequilibrium steered molecular dynamics (SMD) simulations (Fig. S7), which gave similar results to that of previous equilibrium umbrella sampling simulations (32, 34). The deprotonation of NH_4^+ to NH_3 has been proposed to occur when the solute enters the hydrophobic lumen from the periplasmic vestibule (1, 11). For NH_4^+ deprotonation to occur, the pK_a of ammonia inside the channel needs to be lowered below 6.5 (1, 11). Lowering pK_a of ammonia from 9.25 (pK_a in aqueous solution) to 6.5 requires a $\Delta\Delta G$ of 3.76 kcal/mol. Com-

paring the free energy profile of NH_4^+ conduction to that of NH_3 shows the $\Delta\Delta G$ increases above the 3.76 kcal/mol level when the solutes pass through the phenyl rings of the F107/F215 pair (Fig. 1C and Fig. S7). This suggests that NH_4^+ releases its proton (most likely to the bulk of water) as it passes through the phenyl rings' gate, where the energy of NH_4^+ diffusion becomes higher than the energy required for lowering its pK_a from 9.25 to 6.5. This is consistent with previous conclusions based on the calculations of apparent pK_a of ammonia along the transport pathway (32, 34).

Free Energy Profile of CO_2 Conduction by AmtB. CO_2 was reported to be conducted by the members of the Rh/Amt/MEP family (14). Although the free energy profiles of NH_4^+ and NH_3 conduction through AmtB have been calculated by two independent groups (32, 34), the free energy profile for conduction of CO_2 has not been reported. Here the CO_2 conduction was simulated along three monomeric channels using the umbrella sampling method for better understanding of selectivity mechanism of AmtB. The average free energy profile from the three monomers shows four distinct local energy minima along the pathway, so-called CO_2 -1, CO_2 -2, CO_2 -3, and CO_2 -4 (Fig. 2A), which are consistent with that of Am conduction. The location of CO_2 -1 energy minimum matches perfectly with the Am1 site. The CO_2 -2 and CO_2 -3 energy minima are located inside the hydrophobic lumen. CO_2 -2 is located between H168 and H318 and matches with the proposed Am3 site, which is one of the three proposed NH_3 sites

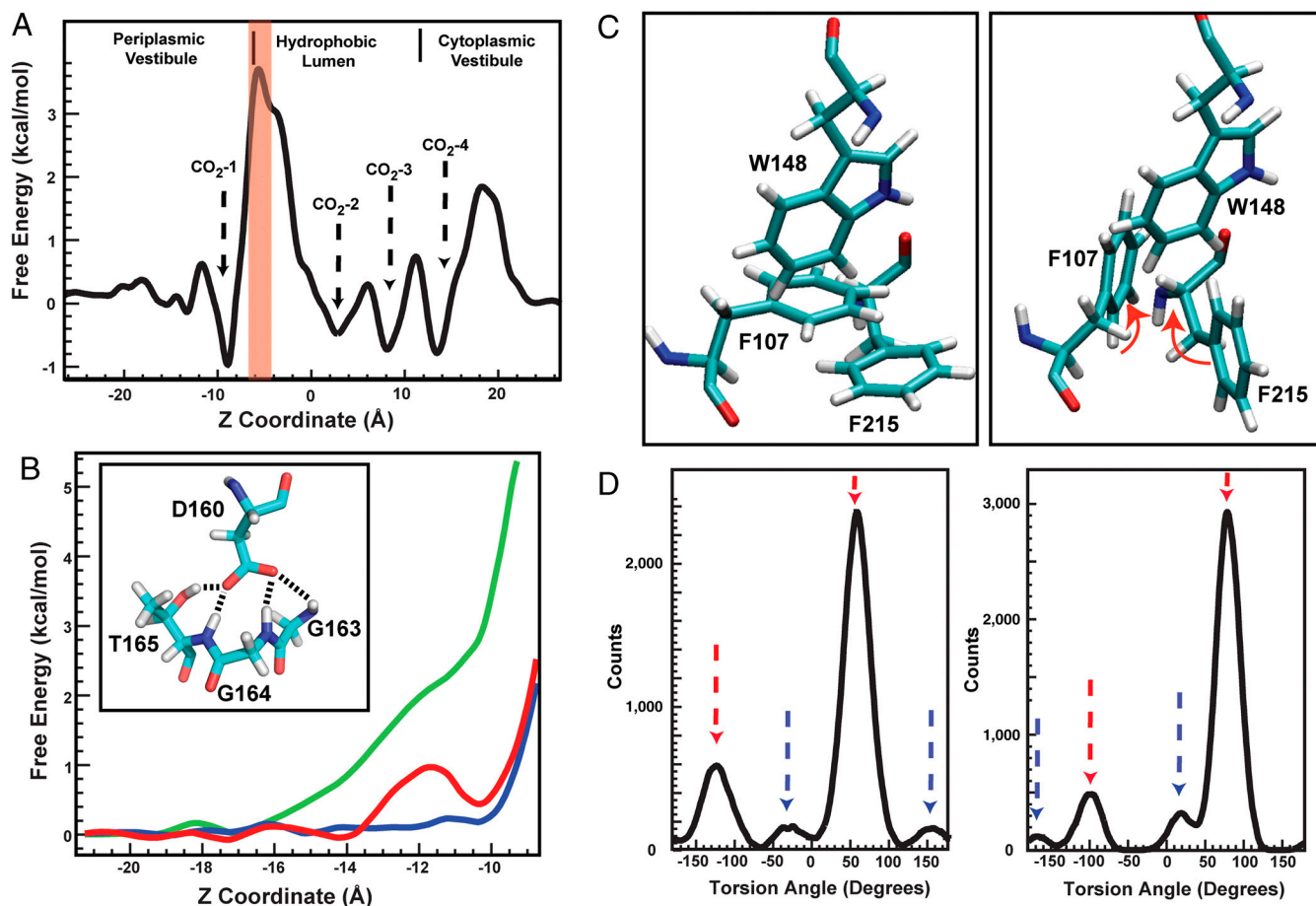


Fig. 2. (A) The free energy profile of CO_2 conduction through AmtB channel calculated using umbrella sampling methods. The energy profile is the average value for three monomers. The regions between the two phenyl rings of F107/F215 are marked by a red rectangle. (B) Free energy profiles of NH_4^+ conduction through native AmtB (red), "neutral D160" with constraints on the atomic distances (Blue), and "neutral D160" with no constraints (Green). (Inset) The four hydrogen bonds between D160 and the residues G163, G164, and T165. (C) The partially stacked phenyl rings of F107 and F215 flip open (Right) and close (Left) simultaneously. The red arrows show the directions of rotations. (D) The distribution of the torsion angles $C_\alpha-C_\beta-C_\gamma-C_{\delta 1}$ for F107 (Left) and F215 (Right). For each residue the torsion angles corresponding with the closed and open states are indicated by red and blue arrows, respectively.

(11). CO₂-3 is located at the bottom of the hydrophobic lumen, right before the F31 gate, and its location also matches with the suggested Am4 proposed NH₃ site (11). To diffuse from the hydrophobic lumen into the cytoplasmic vestibule, CO₂ needs to overcome an energy barrier of 2 kcal/mol. The fourth local free energy minimum on the CO₂ conduction path, CO₂-4, was observed inside the cytoplasmic vestibule. This location matches with the NH₄⁺ binding site, Am-5, proposed to be the NH₃ reprotonation site in the cytoplasmic vestibule (32). In order to diffuse from the cytoplasmic vestibule to the intracellular region, CO₂ needs to overcome an energy barrier of approximately 2.5 kcal/mol.

Interestingly, the derived free energy profile for CO₂ conduction through the hydrophobic lumen is very similar to that of NH₃ (32, 34). This indicates the umbrella sampling free energy profile of CO₂ conduction through the hydrophobic lumen cannot explain the AmtB preference for Am over CO₂. However, as the results of equilibrium MD simulations show, it is instead the periplasmic vestibule that forms a selectivity filter for the channel enabling AmtB to recruit Am in preference to CO₂.

The Role of D160 in Solute Recruitment by Periplasmic Vestibule. The conserved residue D160 is essential for the activity of AmtB (14, 36). However, the precise role of D160 is a controversial topic. The carboxyl oxygen atoms of D160 form four hydrogen bonds with residues G163, G164, and T165 and stabilize the fifth helix and M4-M5 loop (see Fig. 2*B*, *Inset*). Because D160 is not exposed to the periplasmic vestibule in the crystal structure, it was suggested that D160's role should be to stabilize the 3D structure of AmtB (Fig. S3) (11). Two MD simulation reports suggested that D160 is directly involved in the deprotonation process by accepting the proton from NH₄⁺ as it enters the hydrophobic lumen (34, 38). However, other simulations have suggested that D160 is not involved in the deprotonation of NH₄⁺ (32). To gain a better understanding of the role of D160 in solute conduction, we performed a thorough molecular dynamics simulation using the umbrella sampling methods. The goal of this simulation was to determine how the charge on the D160 side chain affects Am conduction through the periplasmic vestibule. Because MD simulations on a single monomer or the trimeric forms have been shown by others to yield similar results (32, 34), in these simulations each monomer was treated as an independent functional channel in the trimeric AmtB. In our simulations, D160 in monomer 1 was kept in the native form with no constraint. In monomers 2 and 3, the charge on the carboxyl group of D160 was neutralized. In addition, in monomer 2 the four hydrogen bonds were mimicked by harmonic constraints on the distances between the atoms (see *Materials and Methods*). These constraints allow us to evaluate the effects of neutralizing the charge of D160 on Am conduction without disturbing the overall structure. Monomer 3 does not carry any constraints; therefore, in this monomer we expect to observe the possible structural effects of removing the charge of D160. The umbrella sampling free energy profiles of NH₄⁺ conduction into the periplasmic vestibule were compared in the three monomers (Fig. 2*B*). Monomers 1 and 2 did not show significant differences in the free energy profile other than the presence of an approximately 0.6 kcal/mol energy barrier in monomer 1 (or native monomer) right above the Am1 site at $z = -12$ Å. The major changes in the free energy profile were observed with monomer 3, which shows a steep increase in the free energy values starting at $z = -16$ Å, where NH₄⁺ approaches the Am1 site (Fig. 2*B*). Between monomer 1 and monomer 3 rmsd analysis suggests the side chain displacements of L159 (rmsd = 3.0 Å), W148 (rmsd = 3.4 Å), and Q104 (rmsd = 3.8 Å) could be responsible for this significant energy barrier in monomer 3. These three residues are located at the periplasmic vestibule (Fig. S3), and their rmsds are clearly higher than the average rmsd for the side chains of all other residues

(calculated to be 1.44). The similarity between the free energy profile of monomer 3 and that of D160A mutant (38) suggests that the structural changes due to the missing hydrogen bonds are responsible for the loss of activity in the D160A mutant (36). On the other hand, the mutation of D177N in RhCG (equivalent to D160N in AmtB) retains 58% of the channel activity (39). Although the mutation of D160N removes the charge on residue 160, Asn can retain some of the hydrogen bonds between the residue 160 and residues G163, G164, and T165. Therefore, it seems D160N mutation does not severely change the overall structure of the vestibule, as compared to the D160A mutant. Overall, our results indicate that D160 plays mainly a structural role in ammonia channels family.

The Synchronized Movement of F107 and F215 Phenyl Rings. The periplasmic vestibule of AmtB is separated from the hydrophobic lumen by the partially stacked phenyl rings of the conserved residues F107 and F215 (Fig. 1*A*). NH₄⁺ is proposed to release its proton as it passes through this gate and enters the hydrophobic lumen (11). However, the functional role of these residues is not completely understood, and there are conflicting reports about the effect of their mutations on channel activities (39, 40). Previous works suggested that F107 is not as essential as F215 for the in vivo activity of AmtB, and the double mutant (F107A, F215A) shows no activity (40). On the other hand, a recent report by Zidi-Yahiaoui et al. shows that mutation of either F130 (equivalent to F107 in AmtB) or F235 (equivalent to F215 in AmtB) inactivates the RhCG channel and the double mutation recovers partial channel activity (39). During the equilibrium MD simulations we observed these rings to adapt two dominant conformations corresponding to the open and closed states of the gate (Fig. 2*C*). In order to understand the role of these residues, we conducted a detailed analysis on their dynamics during the equilibrium MD simulations. The torsion angles of C-C_α-C_β-C_γ and C_α-C_β-C_γ-C_{δ1} (Fig. S8*A*), for both F107 and F215, were recorded every 5 ps during a total of 247-ns simulation for each monomer of the trimeric AmtB, which is equivalent to 740 ns for a single channel. For each torsion angle, we analyzed 148,000 samples. The torsion angle of C-C_α-C_β-C_γ of each phenyl residue shows limited fluctuations around a single angle (the σ of the Gaussian fit for each angle is in parentheses): 158° (±14°) for F107 and 72° (±10°) for F215 (Fig. S8*B*). Therefore, it seems the dynamics of the torsion angle of C_α-C_β-C_γ-C_{δ1} in both F107 and F215 defines the open and closed states of the phenyl rings gate. In the open state, i.e., the vestibule is open to the hydrophobic lumen, the angles are 155° (±20°) or -27° (±20°) in F107 and 20° (±17°) or -166° (±14°) in F215 (Fig. 2*C* and *D*). The angles of 58° (±18°) or -123° (±20°) for F107 and 80° (±16°) or -100° (±15°) for F215 correspond to the closed state, i.e., the entrance of the lumen is blocked (Fig. 2*C* and *D*).

To distinguish between gate opening events and random fluctuations, an opening event was registered only when the rings stay in the open conformation for at least 100 ps (Fig. S9). The phenyl rings simultaneously flip open at least once every 10 ns and stay open for 0.5–4 ns; however, the opening of a single ring lasts less than 0.1 ns. On average, both phenyl rings are observed to be simultaneously in the open state 5.0% of the time. If the opening of the two rings were independent, the probability that the two rings flip open together would be 0.4% (calculated using the probability of being open for each phenyl ring), which is much lower than observed value of 5.0%. Furthermore, the rate and duration of opening events were independent of the presence of NH₄⁺ at the periplasmic vestibule. These findings strongly confirm the coordination between the rings for adapting similar conformational states. The π - π interaction of the partially stacked phenyl rings seems to facilitate synchronized behavior of the two rings. Therefore, the presence of both phenyl rings stabilizes the open state of the gate, and this can explain why the removal of

either residue lowers the activity of RhCG (39). The conditional probability analysis showed when F215 is open, the probability of F107 being simultaneously open is ~ 0.93 . However, if F107 is open the probability of F215 being simultaneously open is ~ 0.68 . This suggests the opening of F215 is more important for simultaneous opening of the phenyl rings. These findings explain the experimental results suggesting F215 is more important than F107 for the activity of AmtB (40).

Performing umbrella sampling simulations while the phenyl rings are constrained in an open state did not yield significant changes on the energy profile of NH_4^+ or NH_3 conduction through phenyl ring regions. This indicates that the phenyl rings are not just simple physical gates, and they are probably involved in the deprotonation mechanism in AmtB. This conclusion is supported by the previous experimental results that removal of both phenyl rings, by double mutations of F107A and F215A, inactivates the channel (39, 40).

Conclusions

Here we have used various molecular dynamics simulations techniques to show the importance of periplasmic vestibule in solute selectivity and conduction in AmtB. Equilibrium MD simulations revealed two highly conserved residues E70 and E225 positioned at the opening of the periplasmic vestibule, along with backbone carbonyl groups of the residues in the periplasmic vestibule, that facilitate the recruitment of NH_4^+ . Furthermore, the periplasmic vestibule prefers NH_4^+ over NH_3 , and this makes the channel even more efficient because NH_4^+ is the major species at the biological pH. The periplasmic vestibule, which prefers Am over CO_2 , plays an important role in the solute selectivity (Am vs. CO_2) in AmtB. The results of umbrella sampling simulations indicate that the conserved residue D160 is important for the structural stability of the periplasmic vestibule.

Two partially stacked phenyl rings of the F107 and F215, separating the periplasmic vestibule from the central hydrophobic lumen, should flip open upon solute passage. The dynamics of these phenyl rings show these two rings flip open in a synchronized manner, with a rate of approximately 10^8 flipping events per second. The role of these phenyl rings could be more than just a physical gate for the solutes; they can also be involved in the process of deprotonation of NH_4^+ as it passes through the rings. Further experimental assays and MD simulations are necessary to explain how these phenyl rings facilitate the deprotonation of NH_4^+ .

Materials and Methods

Model Building. The trimeric AmtB model was based upon the X-ray structure of AmtB at 1.35-Å resolution (Protein Data Bank ID code 1U7G) (11). Three mutations (F68S, S126P, and K255L) and SeMet residues were changed back to their native residues. Hydrogen atoms were added to the structure with XPLOR-NIH (41). The protonation states for each His residue were modeled based on their hydrogen bond environment. POPE was used to create a model of a lipid bilayer with dimensions of $120 \text{ \AA} \times 120 \text{ \AA} \times 39 \text{ \AA}$. Trimeric AmtB was inserted into the center of the lipid bilayer and overlapping POPE molecules were removed. The z axis is aligned in the direction of the hydrophobic pore of AmtB and normal to the lipid bilayer plane. The lipid-protein complex was solvated by adding 25-Å TIP3P (42) water slabs on each side of the lipid bilayer. The initial model used in all simulations contained 142,874 atoms, with dimensions of $120 \text{ \AA} \times 120 \text{ \AA} \times 86 \text{ \AA}$.

All the MD simulations were performed with the NAMD program (43) using the CHARMM27 force field (44, 45). Periodic boundary conditions were applied in all three dimensions. A Langevin thermostat and the Langevin piston model (46) were used to keep the temperature and pressure constant at 310 K and 1 atm, respectively. The van der Waals interaction cutoff was set at 12 Å in conjunction with switching at 8 Å. Full electrostatics was employed using the particle mesh Ewald method (47), with a grid spacing less than 1 Å. All simulations used an integration time step of 1.0 fs. The total charge of the system was neutralized by adding six Cl^- ions.

Equilibrium Molecular Dynamic Simulations. To investigate the diffusion of NH_4^+ , NH_3 , or CO_2 into protein vestibules, separate initial models were built for each solute. In each model, 100 water molecules were replaced with

NH_4^+ , NH_3 , or CO_2 molecules (equivalent to the concentration of 300 mM). The solute molecules were evenly distributed on both sides of the lipid bilayer, at least 10 Å away from the plane of the bilayer (Fig. S1). In the NH_4^+ model, 100 Cl^- ions were added to neutralize the system. Before the long MD simulations, each system was first minimized for 2,000 steps and then equilibrated for 2 ns with no constraints on the system. A total of 84 ns, 80 ns, and 82 ns of MD simulations were performed for NH_4^+ , NH_3 , and CO_2 , respectively.

To determine how AmtB attracts various solutes from the bulk of water, the probability distributions of each solute inside a hypothetical cylinder, perpendicular to the plane of the lipid bilayer, were calculated. The height of the cylinder extended the thickness of the periodic boundary box, and with 70-Å diameter it accommodated the trimeric protein (Fig. S4). The number of solute molecules that appeared inside the cylindrical volume was recorded at every 5-ps frame by monitoring the location of nitrogen atom (for $\text{NH}_4^+/\text{NH}_3$) or carbon atom (for CO_2) of each solute during the MD simulations. The probability distribution curves were derived from the observed number of solute molecules per $\text{ns} \times \text{\AA}^3$ along the axis of the cylinder. For each solute, the total probability distributions within the cylinder were normalized to 100. Because this channel does not conduct water (11), the behaviors of solutes (100 molecules) were compared with that of 100 molecules of water that were randomly selected among all 22,882 water molecules. Because the number of total water molecules was significantly higher than that of the solutes, to improve the statistics, the probability distributions of water molecules were averaged over 10 independent sets of 100 different water molecules. The average standard deviation for the probability distributions of water molecules is less than 10% suggesting that our sampling size was a good representative for the distribution of water molecules. The distributions of solute and water molecules at the vicinity of the protein were compared with those of lipid bilayer. To this end, the solute and water molecule distributions within the cylinder accommodating the protein were compared with those within a similar cylinder that was located away from the protein and contains only the lipid bilayer (Fig. S4).

Equilibrium MD simulation data were used to investigate the dynamics of phenyl rings gate. The conditional probability was defined as $P(\text{F107}_{\text{open}} | \text{F215}_{\text{open}}) = P(\text{F107}_{\text{open}} \cap \text{F215}_{\text{open}}) / P(\text{F215}_{\text{open}})$, where $P(\text{F107}_{\text{open}} | \text{F215}_{\text{open}})$ is the probability of F107 being in the open state given F215 is open, $P(\text{F107}_{\text{open}} \cap \text{F215}_{\text{open}})$ is the probability of both rings being in the open state, and $P(\text{F215}_{\text{open}})$ is the probability of F215 to be open. A similar equation was used to calculate $P(\text{F215}_{\text{open}} | \text{F107}_{\text{open}})$.

Umbrella Sampling Simulations. The umbrella sampling methods were used to investigate the role of D160 on the NH_4^+ recruitment, as well as calculating the free energy profile of CO_2 conduction through AmtB. During umbrella sampling simulations, each monomer was sampled simultaneously with a 0.5-Å window size. In each sampling window, atom coordinates were recorded at every 0.5 ps, for 450 ps. The first 150 ps were used for equilibration and the last 300 ps were defined as the production run. The starting point for each window was determined by the positions of the atoms from the last frame of the previous window. This way sufficient relaxation of the system was assured.

Based on the required sensitivities of the studies, different biasing harmonic potentials with force constants of $10 \text{ kcal}/(\text{mol} \times \text{\AA}^2)$ (for NH_4^+) and $20 \text{ kcal}/(\text{mol} \times \text{\AA}^2)$ (for CO_2) were applied. The solute molecules were restrained only on the z axis and free to move on the xy plane. The data were unbiased and a free energy profile was calculated by using the weighted histogram analysis (WHAM) method (48, 49).

To investigate the role of D160 on the NH_4^+ free energy profile the model was modified. Monomer 1 was kept in native form, whereas in monomers 2 and 3, the total charge on the side chain of D160 was set to zero. In monomer 2, the four hydrogen bonds were mimicked by applying $20 \text{ kcal}/(\text{mol} \times \text{\AA}^2)$ harmonic constraints on the distances between atoms: D160:OD-G163:N (2.1 Å), D160:OD1-G164:N (1.75 Å), D160:OD2-T165:N (1.6 Å), and D160:OD2-T165:O (1.75 Å). The numbers in parenthesis refer to the distances between the atoms in the crystal structure. For monomer 3, no constraints were imposed between atoms.

Steered Molecular Dynamic Simulations. Free energy profile of NH_4^+ and NH_3 diffusions through the AmtB channel were calculated using steered MD simulations (50, 51). The center of mass for each solute was pulled at a constant velocity of 5 Å/ns via a spring with a force constant of 150 pN/Å. For each run the work done (W) was calculated based on the integral of the force applied to the spring as a function of coordinate, z. The average of three independent runs was used to reconstruct the free energy profile based on the Jarzynski's equality (52): $\langle e^{-\beta W} \rangle = e^{-\beta \Delta G}$, where $\beta = 1/k_B T$, k_B is the Boltzmann constant, and T is the temperature.

ACKNOWLEDGMENTS. The authors thank Dr. Adrian Elcock and Dr. Claudio J. Margulis for their valuable discussions, and Dr. Alan Grossfield for sharing his code for WHAM. The authors thank University of Iowa, Carver College of

Medicine for funding. This research was supported in part by the National Science Foundation through TeraGrid resources provided by Texas Advanced Center under Grant TG-MCB100018.

- Khademi S, Stroud RM (2006) The Amt/MEP/Rh family: Structure of AmtB and the mechanism of ammonia gas conduction. *Physiology* 21:419–429.
- Marini AM, Vissers S, Urrestarazu A, Andre B (1994) Cloning and expression of the MEP1 gene encoding an ammonium transporter in *Saccharomyces cerevisiae*. *EMBO J* 13:3456–3463.
- Ninnemann O, Jauniaux JC, Frommer WB (1994) Identification of a high affinity NH_4^+ transporter from plants. *EMBO J* 13:3464–3471.
- Sieve RM, et al. (1996) Functional and genetic characterization of the (methyl)ammonium uptake carrier of *Corynebacterium glutamicum*. *J Biol Chem* 271:5398–5403.
- Marini AM, Urrestarazu A, Beauwens R, Andre B (1997) The Rh (rhesus) blood group polypeptides are related to NH_4^+ transporters. *Trends Biochem Sci* 22:460–461.
- Marini AM, et al. (2000) The human Rhesus-associated RhAG protein and a kidney homologue promote ammonium transport in yeast. *Nat Genet* 26:341–344.
- Liu Z, et al. (2000) Characterization of human RhCG and mouse Rhcg as novel none-rythroid Rh glycoprotein homologues predominantly expressed in kidney and testis. *J Biol Chem* 275:25641–25651.
- Liu Z, Peng J, Mo R, Hui C, Huang CH (2001) Rh type B glycoprotein is a new member of the Rh superfamily and a putative ammonia transporter in mammals. *J Biol Chem* 276:1424–1433.
- Biver S, et al. (2008) A role for Rhesus factor Rhcg in renal ammonium excretion and male fertility. *Nature* 456:339–343.
- Ripoche P, et al. (2004) Human Rhesus-associated glycoprotein mediates facilitated transport of $\text{NH}(3)$ into red blood cells. *Proc Natl Acad Sci USA* 101:17222–17227.
- Khademi S, et al. (2004) Mechanism of ammonia transport by Amt/MEP/Rh: Structure of AmtB at 1.35 Å. *Science* 305:1587–1594.
- Mouro-Chanteloup I, et al. (2010) Functional reconstitution into liposomes of purified human RhCG ammonia channel. *PLoS One* 5:e8921.
- Musa-Aziz R, Jiang L, Chen LM, Behar KL, Boron WF (2009) Concentration-dependent effects on intracellular and surface pH of exposing *Xenopus* oocytes to solutions containing $\text{NH}_3/\text{NH}_4^+$. *J Membr Biol* 228:15–31.
- Musa-Aziz R, Chen LM, Pelletier MF, Boron WF (2009) Relative CO_2/NH_3 selectivities of AQP1, AQP4, AQP5, AmtB, and RhAG. *Proc Natl Acad Sci USA* 106:5406–5411.
- Ludewig U (2006) Ion transport versus gas conduction: Function of AMT/Rh-type proteins. *Transfus Clin Biol* 13:111–116.
- Zheng L, Kostrewa D, Berneche S, Winkler FK, Li XD (2004) The mechanism of ammonia transport based on the crystal structure of AmtB of *Escherichia coli*. *Proc Natl Acad Sci USA* 101(49):17090–17095.
- Andrade SL, Dickmanns A, Ficner R, Einsle O (2005) Crystal structure of the archaeal ammonium transporter Amt-1 from *Archaeoglobus fulgidus*. *Proc Natl Acad Sci USA* 102:14994–14999.
- Conroy MJ, et al. (2007) The crystal structure of the *Escherichia coli* AmtB-GlnK complex reveals how GlnK regulates the ammonia channel. *Proc Natl Acad Sci USA* 104:1213–1218.
- Gruswitz F, O'Connell J, 3rd, Stroud RM (2007) Inhibitory complex of the transmembrane ammonia channel, AmtB, and the cytosolic regulatory protein, GlnK, at 1.96 Å. *Proc Natl Acad Sci USA* 104:42–47.
- Lupo D, et al. (2007) The 1.3-Å resolution structure of *Nitrosomonas europaea* Rh50 and mechanistic implications for NH_3 transport by Rhesus family proteins. *Proc Natl Acad Sci USA* 104:19303–19308.
- Li X, Jayachandran S, Nguyen HH, Chan MK (2007) Structure of the *Nitrosomonas europaea* Rh protein. *Proc Natl Acad Sci USA* 104:19279–19284.
- Gruswitz F, et al. (2010) Function of human Rh based on structure of RhCG at 2.1 Å. *Proc Natl Acad Sci USA* 107:9638–9643.
- Blakey D, et al. (2002) Purification of the *Escherichia coli* ammonium transporter AmtB reveals a trimeric stoichiometry. *Biochem J* 364:527–535.
- Conroy MJ, et al. (2004) Electron and atomic force microscopy of the trimeric ammonium transporter AmtB. *EMBO Rep* 5:1153–1158.
- Kustu S, Inwood W (2006) Biological gas channels for NH_3 and CO_2 : evidence that Rh (Rhesus) proteins are CO_2 channels. *Transfus Clin Biol* 13:103–110.
- Luzhkov VB, Almlof M, Nervall M, Aqvist J (2006) Computational study of the binding affinity and selectivity of the bacterial ammonium transporter AmtB. *Biochemistry* 45:10807–10814.
- Ishikita H (2007) Modulation of the protein environment in the hydrophilic pore of the ammonia transporter protein AmtB upon GlnK protein binding. *FEBS Lett* 581:4293–4297.
- Yang H, Xu Y, Zhu W, Chen K, Jiang H (2007) Detailed mechanism for AmtB conducting $\text{NH}_4^+/\text{NH}_3$: molecular dynamics simulations. *Biophys J* 92:877–885.
- Lamoureux G, Klein ML, Berneche S (2007) A stable water chain in the hydrophobic pore of the AmtB ammonium transporter. *Biophys J* 92:L82–84.
- Ishikita H, Knapp EW (2007) Protonation states of ammonia/ammonium in the hydrophobic pore of ammonia transporter protein AmtB. *J Am Chem Soc* 129:1210–1215.
- Bostick DL, Brooks CL, 3rd (2007) On the equivalence point for ammonium (de)protonation during its transport through the AmtB channel. *Biophys J* 92:L103–105.
- Bostick DL, Brooks CL, 3rd (2007) Deprotonation by dehydration: The origin of ammonium sensing in the AmtB channel. *PLoS Comput Biol* 3:e22.
- Nygaard TP, Rovira C, Peters GH, Jensen MO (2006) Ammonium recruitment and ammonia transport by *E. coli* ammonia channel AmtB. *Biophys J* 91:4401–4412.
- Lin Y, Cao Z, Mo Y (2006) Molecular dynamics simulations on the *Escherichia coli* ammonia channel protein AmtB: Mechanism of ammonia/ammonium transport. *J Am Chem Soc* 128:10876–10884.
- Liu Y, Hu X (2006) Molecular determinants for binding of ammonium ion in the ammonia transporter AmtB-A quantum chemical analysis. *J Phys Chem A* 110:1375–1381.
- Javelle A, Severi E, Thornton J, Merrick M (2004) Ammonium sensing in *Escherichia coli*. Role of the ammonium transporter AmtB and AmtB-GlnK complex formation. *J Biol Chem* 279:8530–8538.
- Wang Y, Cohen J, Boron WF, Schulten K, Tajkhorshid E (2007) Exploring gas permeability of cellular membranes and membrane channels with molecular dynamics. *J Struct Biol* 157:534–544.
- Lin Y, Cao Z, Mo Y (2009) Functional role of Asp160 and the deprotonation mechanism of ammonium in the *Escherichia coli* ammonia channel protein AmtB. *J Phys Chem B* 113:4922–4929.
- Zidi-Yahiaoui N, et al. (2009) Functional analysis of human RhCG: Comparison with *E. coli* ammonium transporter reveals similarities in the pore and differences in the vestibule. *Am J Physiol-Cell Ph* 297:C537–547.
- Javelle A, et al. (2008) Substrate binding, deprotonation, and selectivity at the periplasmic entrance of the *Escherichia coli* ammonia channel AmtB. *Proc Natl Acad Sci USA* 105:5040–5045.
- Schwieters CD, Kuszewski JJ, Tjandra N, Clore GM (2003) The Xplor-NIH NMR molecular structure determination package. *J Magn Reson* 160:65–73.
- Jorgensen WL, Chandrasekhar J, Madura JD, Impey RD, Klein ML (1983) Comparison of simple potential functions for simulating liquid water. *J Chem Phys* 79:926–935.
- Phillips JC, et al. (2005) Scalable molecular dynamics with NAMD. *J Comput Chem* 26:1781–1802.
- MacKerell AD, Jr, et al. (1998) All-atom empirical potential for molecular modeling and dynamics studies of proteins. *J Phys Chem B* 102:3586–3616.
- Schlenkerich M, et al. (1996) An empirical potential energy function for phospholipids: Criteria for parameter optimization and applications. *Biological Membranes: A Molecular Perspective from Computation and Experiment*, eds KM Merz and B Roux (Birkhauser, Boston), pp 31–81.
- Feller SE, Zhang YH, Pastor RW, Brooks BR (1995) Constant pressure molecular dynamics simulation the Langevin piston method. *J Chem Phys* 103:4613–4621.
- Essmann U, et al. (1995) A smooth particle mesh Ewald method. *J Chem Phys* 103:8577–8593.
- Kumar S, Rosenberg J, Bouzida D, Swendsen R, Kollman P (1995) Multidimensional free-energy calculations using the weighted histogram analysis method. *J Comput Chem* 16:1339–1350.
- Roux B (1995) The calculation of the potential of mean force using computer simulations. *Comput Phys Commun* 91:275–282.
- Isralewitz B, Gao M, Schulten K (2001) Steered molecular dynamics and mechanical functions of proteins. *Curr Opin Struct Biol* 11:224–230.
- Jensen MO, Park S, Tajkhorshid E, Schulten K (2002) Energetics of glycerol conduction through aquaglyceroporin GlpF. *Proc Natl Acad Sci USA* 99:6731–6736.
- Jarzynski C (1997) Nonequilibrium equality for free energy differences. *Phys Rev Lett* 78:2690–2693.